MODELLING RADIATIVELY ACTIVE WATER-ICE CLOUDS: IMPACT ON THE THERMAL STRUCTURE AND WATER CYCLE.

J.-B. Madeleine, F. Forget, E. Millour, *Laboratoire de Météorologie Dynamique, CNRS/UPMC/IPSL, Paris*.

The essential role of water-ice clouds in shaping the thermal structure of the martian atmosphere has been long presumed [1] but neglected in GCMs because of the lack of observations and difficulty to predict the evolution of the water cycle in details. Since then, many evidences of the radiative effect of clouds on the Mars climate have become available [2, 3, 4, 5, 6, 7], and this effect has been simulated by GCMs, thanks to the contraint given by the water cycle observations of TES [8]. The radiative effect of clouds is well reproduced in GCMs for a given time of the year, but it appears much harder to simulate this radiative effect on the long-term. Indeed, the radiative effect of clouds strongly modifies the distribution of water vapor, especially in the polar regions, where it tends to reduce the amount of water vapor injected in the atmosphere during the sublimation of the north polar cap.

In this study, we focus on the thermal structure of the LMD/GCM when clouds are radiatively active, and when their properties (particle size and opacity) are in good agreement with the observations. It allows us to assess their role in shaping the temperatures of the planet, understand their radiative effect in detail (section 2), and evaluate the improvement of the predictions (section 3). However, the corresponding water cycle is too dry by ~ 5 pr.μm, and at the time of this writing, this drying out is not clearly explained. The latter will be further described during the conference, which is a good opportunity to further understand it, since it seems to be a robust feature of many models [9].

1 Modeling approach

Interactive dust and water-ice particles are both implemented in the version of the LMD/GCM presented in this abstract. A semi-interactive dust transport scheme predicts the spatial and size distributions of dust. It is called "semi-interactive" because the predicted dust profiles are scaled so that the total column opacity matches the dust opacity observed by TES (for more information, see the companion abstract of Forget et al. [10]). These dust particles serve as condensation nuclei for water-ice cloud formation. The fraction of dust particles involved in cloud formation is unknown, and we therefore adjust the ratio f_c of the total number of dust particles N over the number of condensation nuclei N_c. The mass mean radius of the ice particles computed by the microphysical scheme (see the paragraph 28 of [11]) is then used to compute the effective sedimentation radius, $r_{\text{sed}} = r_c \ (1+\nu_{\text{eff}})^3$, where ν_{eff} is the effective variance of the lognormal distribution, which is also a tunable parameter. These two parameters, f_c and ν_{eff}, are adjusted so that the simulated cloud properties are consistent with the observations. The resulting cloud opacity at 12.1 μm is presented in Fig. 1 (lower panel), and compared to the observed TES opacity (upper panel). The agreement is sufficiently good to evaluate the radiative effect of clouds, and cloud particle sizes are comparable to the TES and OMEGA observations of [12, 13].

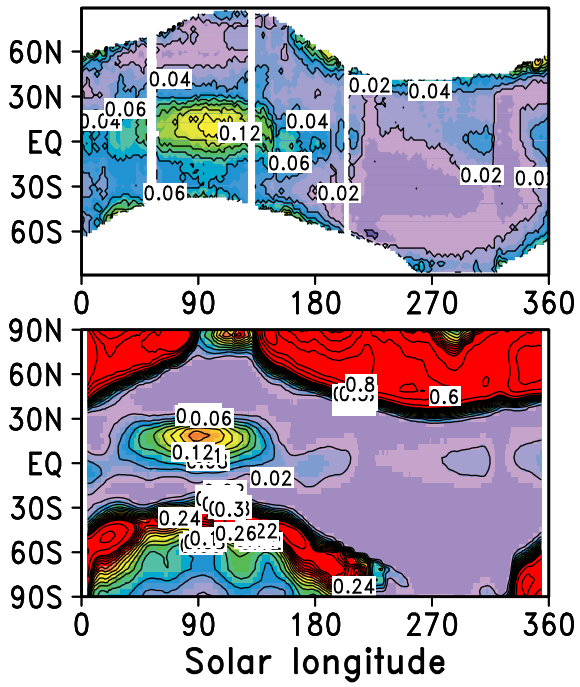

Figure 1: Annual evolution of the zonal mean water-ice opacity at 825 cm^{-1} (12.1 μm, absorption opacity) as retrieved by TES (upper panel) and as simulated by the LMD/GCM (lower panel) for MY26. Contour interval is 0.02. TES cannot retrieve the water-ice opacity in the polar regions, where the GCM predicts thick clouds.

The radiative effect of dust and water-ice particles depends on their single scattering properties, which are a function of the size of the particles. Scattering properties are loaded for different particle sizes in look-up tables, that are generated using the T-Matrix code of [14] and optical indices of Wolff et al. [15] and Warren et al. [16] for dust and water-ice particles, respectively. At each time step, these scattering properties are integrated

over a given size distribution with the effective radius predicted by the GCM in each grid box[1]. We therefore account for the change in scattering due to the differential sedimentation of the dust particles and growth of the water-ice crystals. The radiative transfer codes at solar wavelengths and outside the 15 μm CO_2 band are both based on the two streams algorithm of [17]. Their channels include two solar bands (0.1-0.5 μm and 0.5-5 μm), the silicate band (5-11.5 μm), and the rest of the IR domain (20-200 μm). The net exchange formulation [18] is used in the 15 μm CO_2 band (11.5-20 μm), where scattering by aerosols (dust and ice) is neglected. In this band, only absorption by aerosols is taken into account, and added to that of CO_2 by using $Q_{\rm abs} = Q_{\rm ext}(1-\omega_0)$ [19]. Simulations are run using the dust opacity acquired by TES/MGS during the martian year 26. Resolution is $5.625 \times 3.75^\circ$ in the horizontal (64×48), with 25 levels in the vertical, from the ground to $\sim$ 100 km.

2 Radiative effect of clouds

Before focusing on the global changes induced by radiatively active clouds, we analyzed the changes in temperature over the Tharsis plateau (0°N – 120°W) for a typical day of the L_s = 90°– 120° period. Figure 2.a represents the difference in temperature profiles between two 3D simulations, with and without radiatively active clouds (T_{active}-$T_{inactive}$, contours), and over the course of a day. Black shading indicates the volume mixing ratio of water-ice particles, the maximum value being 250 ppm. Clouds change the temperature mainly by scattering of the infrared radiation, the single scattering albedo being close to one at solar wavelengths. Consequently, clouds tends to heat the atmosphere during the day by absorption of the infrared radiation emitted by the surface, and to cool the atmosphere during the night by infrared emission to space, the surface being colder than the atmospheric layers where clouds form.

This is seen in Fig. 2.a, where the atmosphere is warmed by up to 9 K at $\sim$ 20 km altitude in the afternoon. On the contrary, the atmosphere is cooled by around 6 K below the 10 km level during the night. This nocturnal temperature inversion has been observed by the Radio Science instrument and explained in the light of the GCM simulations of Hinson and Wilson 2004 [4]. In this latter paper, an intensification of the thermal tides by radiatively active clouds is emphasized. This intensification is also evident in Fig. 2.a, where the vertical propagation of the wavenumber one diurnal component is apparent in the temperature field with a wavelength of about 30 km.

To separate radiative and dynamical responses, we performed 1D simulations in the same conditions as the

[1]The effective variance is kept constant and equal to 0.3 and 0.1 for dust and water-ice particles, respectively.

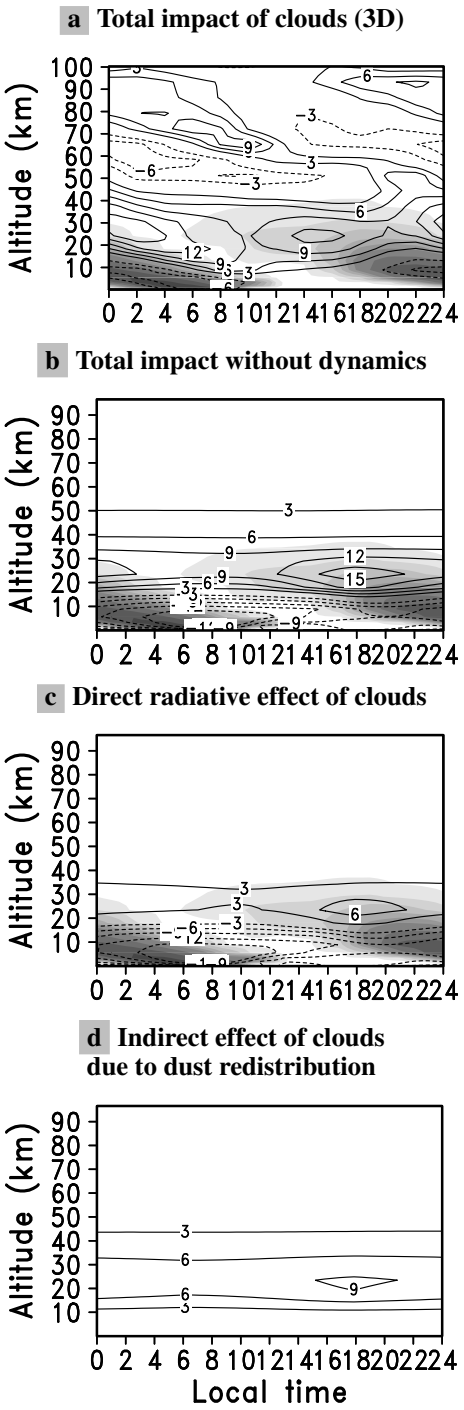

Figure 2: (a) Temperature difference (T_{active}-$T_{inactive}$, contour interval of 3 K) between two simulations, with and without radiatively active clouds, for a typical day of the L_s = 90-120° period, and over the Tharsis plateau. Darker shades indicate higher water-ice volume mixing ratio, the maximum value being 250 ppm. (b) Same as (a), but the 1D version of the GCM is used, and constrained by the dust and water-ice profiles of the 3D simulation. (c) Same as (b), but the dust profile is the same for the two simulations. (d) Temperature difference resulting from the change in the vertical distribution of dust only.

3D simulations, using the dust and water-ice profiles extracted from the 3D simulation. Figure 2.b is the 1D equivalent of Fig. 2.a, and a comparison of the two figures shows that during the night, thermal tides tend to increase the temperature changes induced by radiatively active clouds, whereas the contrary is true during the afternoon. Moreover, we have noticed that radiatively active clouds, by increasing daytime temperatures, favor vertical mixing of the dust layer, resulting in an indirect additional warming near 30 km altitude. This is illustrated by Fig. 2.d, in which the temperature change induced by the vertical mixing of dust alone is represented. The direct radiative effect of clouds is shown in Fig. 2.c. Interestingly, the temperature increase near the 30 km level is mainly due to the vertical redistribution of dust. For example, at 4 PM, dust mixing increases the temperature by $\sim$ 9 K, versus 6 K for clouds. However, the nighttime cooling below the 10 km level is mainly due to the radiative effect of clouds. Above the 10 km level, nighttime temperature is increased by dust redistribution first, and then by the radiative effect of clouds and the adiabatic heating of the thermal tides, the two latter having a similar impact of $\sim$ 3 K.

3 Global temperature changes induced by clouds

After analyzing the radiative effect of clouds, we focused on their global impact on the thermal structure of the atmosphere. This is represented in the upper panel of Fig. 3 (colors), along with the zonal mean water-ice volume mixing ratio in ppm (contours). Three main effects are visible. Near the equator, clouds tends to warm the atmosphere near the 0.5 hPa pressure level, and to cool the atmosphere near 1 hPa. It is especially visible at L_s = 0 – 30°. Then, low-lying clouds cool the atmosphere at both poles, as clearly seen at equinoxes. Finally, by warming the atmosphere near the 0.5 hPa pressure level, clouds increase the meridional temperature gradient and intensify the Hadley cell circulation. This results in an increased adiabatic warming in the descending branch of the Hadley cell, which is visible at all seasons in mid-latitudes, especially during the aphelion cloud season (L_s = 90 – 120° period). It is worth noting that after L_s = 150°, clouds still increase the equatorial temperature by more than 10 K near the 0.5 hPa pressure level, despite their low opacity ($\sim$ 0.02 at 12.1 μm, see Fig. 1).

The GCM temperatures are compared to the TES observations in the lower panel of Fig. 3. The results of the GCM are significantly improved in the tropics, where clouds tend to warm the atmosphere. This is especially visible for the L_s = 90 – 120° period. Indeed, in the ±60° latitude band and near the 0.5 hPa pressure level, the GCM was underestimating temperature by $\sim$ 10 K when clouds were radiatively inactive, as illustrated by the Fig. 2.b of Wilson et al. 2008 [6]. This cold bias of the GCM almost disappears in Fig. 3, except at high altitude, at the 0.1 hPa pressure level.

This is further illustrated in Fig. 4 which shows the daytime (2 PM) equatorial temperature at the 0.5 hPa pressure level observed by TES (+ crosses) and the temperature simulated by the GCM using different configurations: a prescribed dust depth and inactive water-ice clouds in green, the semi-interactive dust scheme without active clouds in red, and both interactive dust and water-ice particles in blue. When clouds become radiatively active, temperatures are increased at almost all seasons, and are closer to the observations. This is especially evident at the aphelion cloud season, during which the cold bias of $\sim$ 10 K disappears. Temperatures are also improved at equinoxes in both polar regions (see the lower panel of Fig. 3). Indeed, if clouds are not active, temperatures are higher than observed by $\sim$ 10 K near the 1 hPa pressure level. Finally, the mid-latitude temperatures are closer to the observations, due to the enhanced adiabatic warming in the descending branch of the Hadley cell.

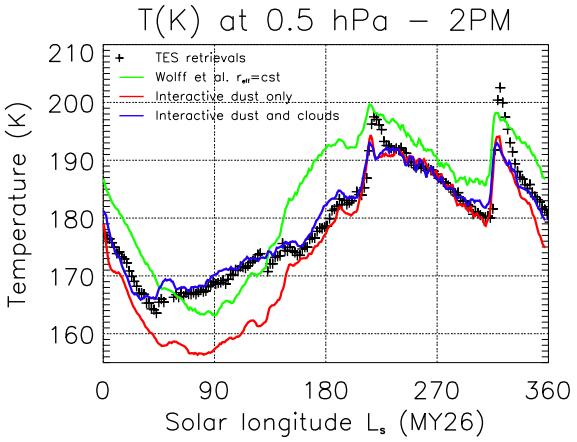

Figure 4: Equatorial temperature at 2 PM for the 0.5 hPa pressure level as measured by TES (+ crosses), and as predicted by the LMD/GCM, without the semi-interactive dust scheme (green), with the semi-interactive dust scheme (red), and with both the semi-interactive dust scheme and the radiatively active water-ice clouds (blue). The agreement is much better when clouds are active, especially around L_s = 90°.

However, some differences remain, mainly at high latitudes. For example, the lower atmosphere of the north polar region is too cold by $\sim$ 15 K during the L_s = 0 – 30° period. Later, between L_s = 90° and L_s = 120°, a warm bias occurs above 60°N near the 0.5 hPa pressure level. Interestingly, this warm bias is mainly explained by the effects of clouds forming at these altitudes (see the upper panel of Fig. 3). Consequently, these clouds are probably thinner in reality than in the model, which might be due to the scavenging of dust nuclei by water-ice clouds. In the winter hemisphere, a cold bias caused

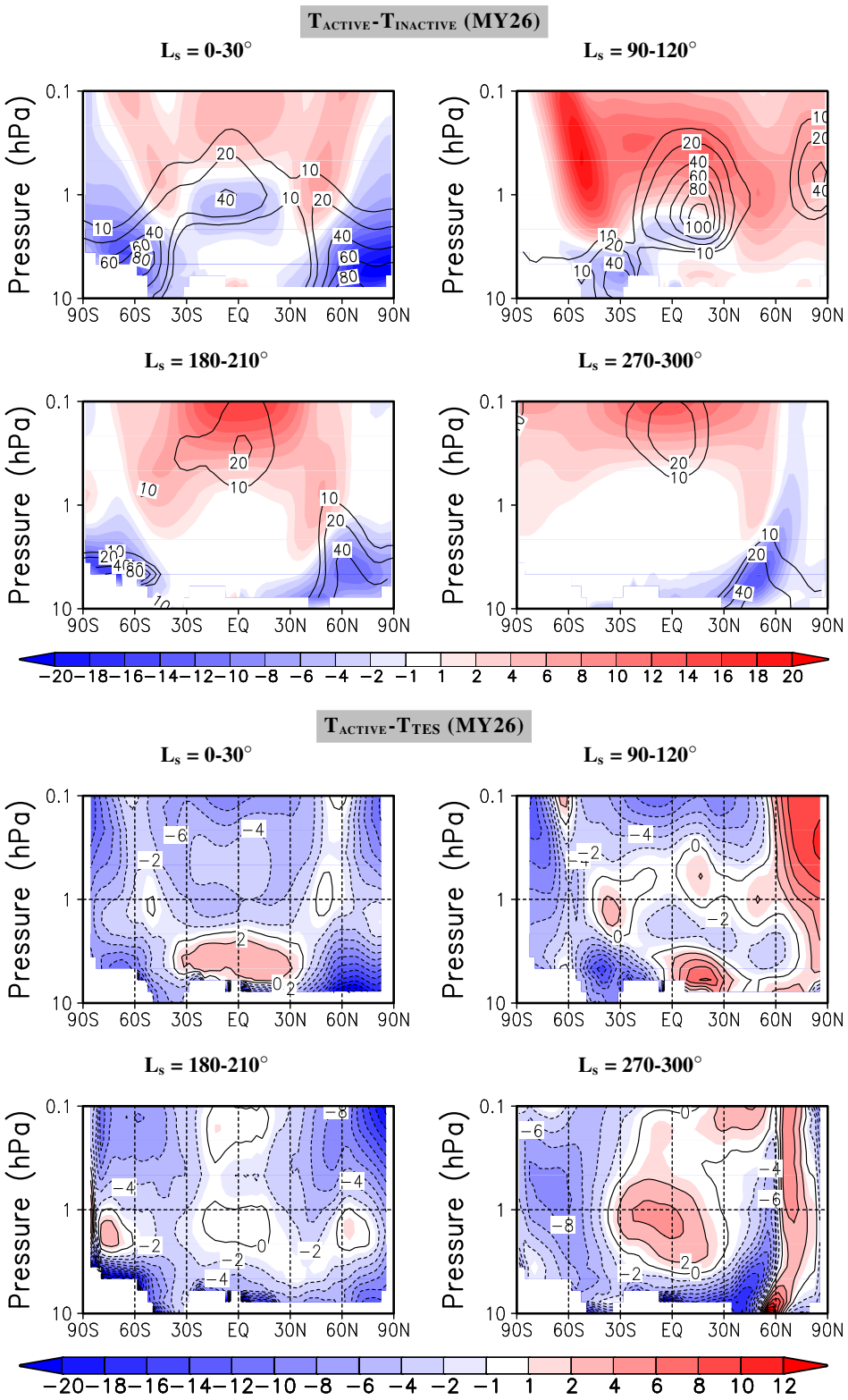

Figure 3: **Upper panel:** Zonal mean temperature difference between two simulations, with and without radiatively active clouds, for four periods. Red shade corresponds to a net warming by clouds. Water-ice volume mixing ratio is represented by contours, in ppm. **Lower panel:** Zonal mean temperature difference between a GCM simulation that includes radiatively active clouds and the TES retrievals of [8] for MY26. Contour interval is 2 K.

by clouds is also apparent in the lower atmosphere near 30°S. Similarly, for the L_s = 270 – 300° period, a cold bias of $\sim$ 10 K appears in the lower atmosphere at 30°N, and is also created by the radiative effect of clouds (upper panel of Fig. 3). Therefore, clouds do not seem to be well predicted in the polar regions at solsticial seasons. Many other biases are beyond the focus of this abstract, for example near perihelion, because they seem to result from an incomplete representation of the dust cycle in our simulations, where a constant lifting rate is assumed.

It is finally worth noting that the TES retrievals of temperature are being refined using a new radiative transfer model (see the abstract of Hoffman et al. in this issue [20]). This new dataset modifies temperature in the polar regions, and at the equator near the 0.1 hPa pressure level. Therefore some biases seen in Fig. 3 may also come from the observations.

4 Conclusions

Radiatively active clouds play a major role in shaping the thermal structure of the Mars atmosphere, and their effect is noticeable at all seasons. Taking their radiative effect into account significantly improves the temperature predictions, but also modifies the water cycle, especially in the polar regions, where the simulated temperatures and water vapor amounts differ from the observations. Further analysis of the polar regions is thus required, along with a better understanding of the physical processes, as scavenging of dust particles, that are currently missing in our model.

References

[1] F. M. Flasar and R. M. Goody, "Diurnal behaviour of water on Mars," *Planetary and Space Science*, vol. 24, pp. 161–181, Feb. 1976.

[2] R. M. Haberle, M. M. Joshi, J. R. Murphy, J. R. Barnes, J. T. Schofield, G. Wilson, M. Lopez-Valverde, J. L. Hollingsworth, A. F. C. Bridger, and J. Schaeffer, "General circulation model simulations of the Mars Pathfinder atmospheric structure investigation/meteorology data," *Journal of Geophysical Research*, vol. 104, pp. 8957–8974, Apr. 1999.

[3] A. Colaprete, O. B. Toon, and J. A. Magalhães, "Cloud formation under Mars Pathfinder conditions," *Journal of Geophysical Research*, vol. 104, pp. 9043–9054, Apr. 1999.

[4] D. P. Hinson and R. J. Wilson, "Temperature inversions, thermal tides, and water ice clouds in the Martian tropics," *Journal of Geophysical Research (Planets)*, vol. 109, pp. 1002–+, Jan. 2004.

[5] R. J. Wilson, G. A. Neumann, and M. D. Smith, "Diurnal variation and radiative influence of Martian water ice clouds," *Geophysical Research Letters*, vol. 34, p. L02710, Jan. 2007.

[6] R. Wilson, S. Lewis, L. Montabone, and M. Smith, "Influence of water ice clouds on Martian tropical atmospheric temperatures," *Geophys. Res. Lett*, vol. 35, 2008.

[7] A. Colaprete, J. R. Barnes, R. M. Haberle, and F. Montmessin, "CO2 clouds, CAPE and convection on Mars: Observations and general circulation modeling," *Planetary and Space Science*, vol. 56, pp. 150–180, Feb. 2008.

[8] M. D. Smith, "Interannual variability in TES atmospheric observations of Mars during 1999-2003," *Icarus*, vol. 167, pp. 148–165, Jan. 2004.

[9] R. M. Haberle, F. Montmessin, M. A. Kahre, J. L. Hollingsworth, J. Schaeffer, M. J. Wolff, and R. J. Wilson, "Radiative Effects of Water Ice Clouds on the Martian Seasonal Water Cycle," in *Mars Atmosphere Modelling and Observations (this issue)*, Feb. 2011.

[10] F. Forget and the LMD/GCM team, "Toward a new generation LMD general circulation model," in *Mars Atmosphere Modelling and Observations (this issue)*, Feb. 2011.

[11] F. Montmessin, F. Forget, P. Rannou, M. Cabane, and R. M. Haberle, "Origin and role of water ice clouds in the Martian water cycle as inferred from a general circulation model," *Journal of Geophysical Research (Planets)*, vol. 109, p. E10004, Oct. 2004.

[12] M. Wolff and R. Clancy, "Constraints on the size of Martian aerosols from Thermal Emission Spectrometer observations," *Journal of Geophysical Research*, vol. 108, no. E9, p. 5097, 2003.

[13] J.-B. Madeleine, F. Forget, A. Spiga, M. Wolff, F. Montmessin, M. Vincendon, D. Jouglet, B. Gondet, J.-P. Bibring, Y. Langevin, and B. Schmitt, "Aphelion water-ice cloud mapping and property retrieval using the OMEGA/MEx imaging spectrometer," in *Mars Atmosphere Modelling and Observations (this issue)*, Feb. 2011.

[14] M. I. Mishchenko, L. D. Travis, and D. W. Mackowski, "T-matrix computations of light scattering by nonspherical particles: a review.," *Journal of Quantitative Spectroscopy and Radiative Transfer*, vol. 55, pp. 535–575, May 1996.

[15] M. J. Wolff, M. D. Smith, R. T. Clancy, R. Arvidson, M. Kahre, F. Seelos, S. Murchie, and H. Savijärvi, "Wavelength dependence of dust aerosol single scattering albedo as observed by the Compact Reconnaissance Imaging Spectrometer," *Journal of Geophysical Research (Planets)*, vol. 114, p. E00D04, June 2009.

[16] S. G. Warren, "Optical constants of ice from the ultraviolet to the microwave," *Applied Optics*, vol. 23, p. 1206, Apr. 1984.

[17] O. B. Toon, C. P. McKay, T. P. Ackerman, and K. Santhanam, "Rapid calculation of radiative heating rates and photodissociation rates in inhomogeneous multiple scattering atmospheres," *Journal of Geophysical Research*, vol. 94, pp. 16287–16301, Nov. 1989.

[18] J.-L. Dufresne, R. Fournier, C. Hourdin, and F. Hourdin, "Net Exchange Reformulation of Radiative Transfer in the CO_2 15-μm Band on Mars.," *Journal of Atmospheric Sciences*, vol. 62, pp. 3303–3319, Sept. 2005.

[19] F. Forget, F. Hourdin, R. Fournier, C. Hourdin, O. Talagrand, M. Collins, S. R. Lewis, P. L. Read, and J.-P. Huot, "Improved general circulation models of the Martian atmosphere from the surface to above 80 km," *Journal of Geophysical Research*, vol. 104, pp. 24155–24176, Oct. 1999.

[20] M. J. Hoffman, J. Eluszkiewicz, R. Hoffman, S. J. Greybush, E. Kalnay, and R. J. Wilson, "Evaluation of an optimal spectral sampling retrieval algorithm for thermal emission spectrometer radiances," in *Mars Atmosphere Modelling and Observations*, Feb. 2011.